

## THE INITIAL MASS FUNCTIONS OF FOUR EMBEDDED STELLAR CLUSTERS

A. LEISTRA<sup>1</sup>, A. S. COTERA<sup>2</sup>, J. LIEBERT<sup>1</sup>

*Draft version November 17, 2018*

### ABSTRACT

We present near-infrared  $J$ ,  $H$ , and  $K$  images of four embedded stellar clusters in the Galaxy. We find a significant fraction of pre-main-sequence stars present in at least one of the clusters. For the clusters dominated by main-sequence stars, we determine the initial mass function (IMF) both by using the  $K$  luminosity function and a global extinction correction and by deriving individual extinction corrections for each star based on their placement in the  $K$  vs.  $H - K$  color-magnitude diagram. Based on our IMFs we find a significant discrepancy between the mean IMF derived via the different methods, suggesting that taking individual extinctions into account is necessary to correctly derive the IMF for an embedded cluster.

*Subject headings:* open clusters and associations: general — stars: formation — stars: luminosity function, mass function

### 1. INTRODUCTION

Embedded clusters are increasingly recognized as vital sites of star formation for both low- and high-mass stars. Recent studies indicate that clusters may account for 70-90% of star formation and that embedded clusters (those still partially or fully enshrouded in their natal molecular cloud) may exceed the number of older, non-embedded open clusters by a factor of  $\sim 20$  (Elmegreen et al. 2000; Lada & Lada 2003). The stellar content of embedded clusters within well-known star formation regions can now be probed, where high extinction ( $A_V \gtrsim 10$ ) prohibits studies at optical wavelengths. The IMF of such clusters has generally been found to be consistent with a Salpeter value with a slope of  $\Gamma = -1.35$  (e.g. Okumura et al. 2000; Blum, Daminieli, & Conti 2001; Figuerêdo et al. 2002) although outliers have been found as well, generally with flatter slopes than the Salpeter value (e.g. Porras et al. 1999).

Although near-infrared (NIR) spectral classification of massive stars is possible (Hanson et al. 1996), in most cases determinations of the IMF from NIR data rely heavily, if not exclusively, on photometry and use spectroscopy only to obtain reliable masses of the few brightest and most massive stars in a cluster if at all. Since these results thus depend on stellar evolutionary models as well as details of the handling of extinction, this raises concerns about to what extent the IMF depends on the methodology employed. Massey (2003) cites the example of NGC 6611, where two separate analyses of the same data (Hillenbrand et al. 1993; Massey et al. 1995) using different treatments of extinction produced IMFs differing by more than the formal  $1\sigma$  errors would suggest ( $\Gamma = -1.1 \pm 0.1$  and  $\Gamma = -0.7 \pm 0.2$ .) Similarly, the IMF for the G305+0.2 embedded cluster differs by more than the errors between the value derived from the  $K$  luminosity function (KLF;  $\Gamma = -1.5 \pm 0.3$ ) and that derived using the color-magnitude diagram ( $\Gamma = -0.98 \pm 0.2$ )

(Leistra et al. 2005). Claims that variations in the IMF exist, whether based on individual extreme clusters such as the Arches or a general analysis of the data (Scalo 1998), must thus be handled with care to compare only results based on similar methodology.

The final release of the Two Micron All Sky Survey (2MASS) has fostered studies (e.g. Dutra & Bica 2000, 2001; Bica et al. 2003; Ivanov et al. 2002) which can probe a much larger portion of the Galaxy for previously unknown embedded stellar clusters and significantly increased the number of known embedded clusters. A compilation of some of these results along with previously known embedded clusters is presented in Porras et al. (2003) who find that  $\sim 80\%$  of the stars in their sample are found in “large clusters” of more than 100 stars, despite the rarity of such clusters. However, these studies are not foolproof, and compilations of “embedded clusters” based purely on the 2MASS data without followup must be treated with caution. The studies based solely on stellar density criteria (e.g. Dutra & Bica 2000, 2001) have been found in followup work by different groups (e.g. Dutra et al. 2003; Leistra et al. 2005; Borissova et al. 2005) to have only about a 50% success rate toward the inner Galaxy where the stellar background is high. We have performed an independent search of the 2MASS archive, searching the Point Source Catalog for regions of higher stellar density than the background (determined locally within a  $5'$  radius) which are redder in  $H - K$  than the local field. This selects for embedded clusters, with the color criteria helping to eliminate chance superpositions and regions of low extinction. A large background radius and the use of color selection are critical to the automated identification of embedded clusters, but even color selection can fail in regions of high background stellar density, where patchy extinction can mimic clusters.

In §2 we present the observations and data reduction for four embedded clusters found in the 2MASS Point Source Catalog, in §3 we present the  $K$ -band luminosity functions (KLF) and initial mass functions (IMF) for the clusters, and in §3.5 we address the issue of systematic differences between different methods of deriving the IMF for embedded clusters, for our clusters as well as

<sup>1</sup> Steward Observatory, University of Arizona, 933 N. Cherry Ave., Tucson, AZ 85721

<sup>2</sup> SETI Institute, 515 N. Whisman Road, Mountain View, CA 94043

Electronic address: aleistra@as.arizona.edu, acotera@seti.org, jliebert@as.arizona.edu

IMFs from the literature.

## 2. OBSERVATIONS & DATA REDUCTION

We selected five young stellar cluster candidates from the 2MASS Point Source Catalog based on color and density criteria as described in (Leistra et al. 2005). We selected regions with a higher stellar density than the locally defined field with redder  $H - K$  color than the field to select embedded cluster candidates. The cluster candidates were observed using the PISCES instrument (McCarthy et al. 2001) on the 6.5m MMT on Jan10-11, 2003. PISCES uses a 1024x1024 HAWAII array with a platescale of  $0''.185/\text{pixel}$  on the MMT, providing a  $3' \times 3'$  field of view. Images of all cluster candidates were obtained in  $J$ ,  $H$ , and  $K$  filters to a limiting magnitude of  $J = 19.5$ ,  $H = 18.5$ ,  $K = 18$ . Four of our candidates (all except the one near Sh 2-217) were independently identified as cluster candidates by Bica et al. (2003), who used criteria based only on stellar density without color considerations. Our deeper, higher-resolution images suggest that four of these candidates are genuine stellar clusters, while the fifth, near Sh 2-258, contains only a few stars in the PISCES images and could be either a very small cluster or a chance superposition. We present our results for the four confirmed clusters in this paper. Seeing conditions when the images were obtained were variable, ranging from  $0''.5$  to  $1''.1$  at  $K$ .

All images were reduced and combined using IRAF routines. The distortions of the PISCES camera were mapped by imaging the globular cluster NGC 4147 and mapping the observed locations to the USNO-B known coordinates, then constructing a transformation function using the IRAF task *geomap* and correcting the images using IRAF *geotran*. There are too few USNO-B stars in the heavily extinguished regions we observed to provide suitable distortion corrections from the fields themselves. The individual images, taken with a spiral dither pattern, were then combined. We fit a PSF to each image using the IRAF task *psf*, allowing the PSF to vary across the field to compensate for residual distortions. Photometry was then done using IRAF-DAOPHOT.

Photometric calibration was performed using the 2MASS magnitudes of field stars. Stars used for calibration were selected to be well-separated from other stars and from nebulosity in the PISCES images to ensure that they were uncontaminated in the lower-resolution 2MASS images, and to have magnitudes bright enough to have good photometry in 2MASS ( $K < 14$ ). We chose to use a relatively large number of calibration stars rather than selecting the few most isolated stars to reduce effects of potential variability and photometric outliers among the calibration stars. The scatter in the photometric calibration derived from comparison to 2MASS is the dominant source of photometric error, contributing two to three times the measurement errors as reported by DAOPHOT. DAOPHOT errors were  $\sim 0.03$  magnitudes while the calibration uncertainties were  $\sim 0.1$  magnitudes. Quoted errors in the 2MASS photometry were negligible, with most stars having an error of  $\pm 0.003$  mag or less in all bands. Thus, the quoted error should be considered an overestimate when considering the *relative* photometry of stars within either cluster; the calibration errors from comparison to the 2MASS photometry will shift all our measurements by the same amount. No

trend with location on the chip was observed in the calibration for any of the clusters, though the scatter between the PISCES and 2MASS magnitudes becomes significant in the outermost  $15''$ ; we thus exclude these sources from the analysis.

## 3. ANALYSIS

### 3.1. Sh 2-217 Cluster

We present a  $K$ -band image of the cluster near Sh2-217 in Figure 1. The cluster is nearly circular in projection and is quite dense; even in the highest-resolution individual pointings we obtained it suffers from crowding in the central regions. The cluster extends over most, if not all, of the field of view. We present the  $K$  image rather than a color frame because the seeing was significantly better at  $K$ .

This cluster was analyzed in the NIR by Deharveng et al. (2003), who discuss the large uncertainties in the distance to Sh2-217. Based on the Lyman continuum fluxes from the main exciting star of Sh2-217 (located several arcminutes outside our field of view; the cluster is located on the periphery of the H II region) they adopt a distance of  $5.0 \pm 0.8$  kpc., which is consistent with the kinematic distance to the associated molecular gas. The cluster is coincident with a peak in the  $8 \mu\text{m}$  emission as measured by the MSX mission, suggesting dust is still present in the cluster.

The  $K$  vs  $H - K$  color-magnitude diagram is shown in Figure 2. The stellar density (determined in  $K$  where the seeing was best) does not plateau in the  $3' \times 3'$  field of view, suggesting that the true field-star density level has not been reached, and cluster stars are still present out to the edges of the field. As a result, in order to correct for foreground contamination, we selected an adjacent field of the same size from 2MASS to use as a comparison field. We assumed the luminosity function of the field to be the same as that of the outer portions of the cluster (excluding the inner regions to minimize the results of crowding and mass segregation) in order to extrapolate from the limiting magnitude of 2MASS to that of our images. We then binned the field stars by  $K$  and  $H - K$  with a bin size of 0.5 magnitudes and randomly selected the appropriate number of stars for removal from each bin in the cluster region. This is similar to the procedure employed by, among others, (Blum et al. 2000) (who do not describe an extinction correction; this lack of correction is equivalent to assuming a common extinction) and Figueredo et al. (2002), and is the method we employed in (Leistra et al. 2005). The resulting statistically corrected CMD is shown in Figure 3. A total of 62 stars were removed in this procedure, out of an initial total of 236. The fairly wide distribution in  $H - K$  for cluster stars is likely due to a combination of factors, notably an actual spread due to differential extinction to different regions of the cluster and to the greater influence of crowding in  $H$  (where the seeing was poorer). Although we find that individually correcting extinctions generally provides a superior estimation of the IMF compared with using only the  $K$  data and a single extinction for the cluster as a whole, in this situation the lower quality (in particular the poorer seeing and consequently more severe crowding) of the  $H$ -band data leads us expect that the  $K$  luminosity function (KLF) will produce a better

estimate of the IMF for this cluster than the CMD will. We have previously compared these two methods of determining the IMF for embedded clusters in Leistra et al. (2005); in that case, we found they gave different results, with the ‘‘CMD’’ method (which we anticipate will be more reliable in most cases, especially where variable extinction is present) yielding a flatter slope.

### 3.1.1. *The KLF*

In order to obtain a robust determination of the KLF and the IMF, we need to determine the completeness of our data. To do this, we performed artificial star tests. We inserted five artificial stars, each of the same magnitude, at a time into the cluster region, then ran IRAF-DAOPHOT with the same parameters as we used for the initial analysis. This procedure was repeated 50 times for each magnitude bin ( $\Delta m = 0.5$ ), for a total of 250 artificial stars added in each bin in  $H$  and in  $K$ . The stars were added in small numbers at a time to avoid having the artificial stars significantly change the crowding characteristics and thus influence the completeness. The artificial star tests indicate a high level of completeness down to  $K = 17.5$ . The actual completeness is most likely slightly lower, since in the crowded central region of the cluster our method may produce false positives when the artificial star is placed on top of a real star of approximately the same magnitude. Despite this concern we have used the calculated incompleteness in correcting the KLF; however, we have excluded the  $K = 17.5$  bin from consideration, both because this effect will be most pronounced at faint magnitudes, and because statistical uncertainties in the incompleteness will be significant.

Knowing our incompleteness, we can calculate the KLF for the cluster. Figure 4 shows both the uncorrected and completeness-corrected versions of the KLF, as derived from all sources detected in  $K$ . The slope of the KLF is  $0.31 \pm 0.04$ , with no extinction correction applied.

### 3.1.2. *The IMF*

We derived an IMF for the Sh 2-217 cluster by two methods. For both methods we used a distance to the cluster of 5 kpc (Deharveng et al. 2003). In general we believe that the ‘‘CMD method’’ for deriving the IMF, which uses individually-derived extinctions for each star in the cluster, to be more reliable than the ‘‘KLF method’’ which assumes a common extinction to all stars in the cluster, since variable extinction is frequently apparent in the NIR images of embedded clusters. However, in this case our  $K$  data is superior to our  $H$  data due to the difference in the seeing, which was  $\sim 0.''$  in  $K$  and  $\sim 1.2''$  in  $H$ . This suggests that despite the general drawbacks of the KLF method it may be preferable in this situation; including the  $H$ -band data adds nothing if it is of poor quality. At the least, using both methods will provide information on potential systematic effects in the IMF determination that depend on the methodology used.

The KLF method of determining the IMF is sometimes employed even when multi-color photometry and spectra are available (e.g. Blum et al. 2000), and is simply a transformation from  $K$  magnitude bins to mass bins. The major problem with this is that of variable extinction, which for many embedded clusters is significant

even in  $K$ . To make this transformation, we first correct the observed  $K$  for distance and extinction. Without spectra, we cannot obtain a precise estimate for the extinction; instead, we compute an average extinction correction based on the observed  $J - H$  and  $H - K$  colors of the brighter stars. Since there is little difference in the intrinsic  $H - K$  color of stars of spectral type F5 and earlier, this estimate of an average extinction is not sensitive to minor errors in the distance estimate. Using the stellar evolutionary models of Meynet & Maeder (2003) for solar metallicity, we relate the mass for each track to an absolute  $K$  magnitude for a star on the ZAMS. We transformed  $L_{bol}$  to  $K$  using the bolometric corrections from Vacca, Garmany, & Shull (1996) for the early spectral types and Malagnini et al. (1986) for later spectral types. We then use the intrinsic  $V - K$  colors from Bessell & Brett (1988) for A-M stars and from Wegner (1994) for O and B stars. Finally we interpolate linearly between the masses available on the evolutionary tracks to find the masses corresponding to our magnitude bins, and fit a power law to the resulting mass function. The IMF slope we derive by this method is  $\Gamma = -2.7 \pm 0.25$ , excluding bins corresponding to  $K > 17.5$  where incompleteness becomes significant. The slope we fit to the KLF itself for sources detected in both  $H$  and  $K$  is  $0.35 \pm 0.04$ .

We have previously used multi-color photometry in conjunction with near-IR spectroscopy of the brightest stars to determine the IMF for embedded clusters (Leistra et al. 2005). Although we do not have spectra in this case, we can still derive extinctions for individual stars based on their near-IR colors. We use the same evolutionary models and conversions from theoretical to observed quantities described for the KLF method. The ZAMS derived from the evolutionary tracks of Meynet & Maeder (2003) is overplotted on the distance and extinction-corrected CMD in Figure 5. The ZAMS lies in the middle of the distribution of stars due to the method used to estimate an average extinction. The scatter around the ZAMS is rather large, and is likely due to a combination of variable extinction in the cluster region and poor photometry in  $H$ , especially in the central portion of the cluster.

Since extinction appears to vary across the cluster, we impose an extinction limit on the sample used for the CMD computation of the IMF. Since the most massive stars can be seen to greater extinction than less massive stars, neglecting to impose this constraint will produce an overly flat IMF. Thus we need to simultaneously limit our sample by extinction and by mass. We use a mean extinction to the Sh2-217 cluster of  $A_V = 9$  mag as determined by individually de-reddening sources until they reach the main sequence. With the exception of a few extreme outliers that most likely suffer from poor photometry, most sources with higher extinctions have  $A_V < 15$ . At a distance of 5 kpc with our limiting magnitudes, we can observe stars earlier than G4 to an extinction of 9 mag and earlier than F0 to an extinction of 15 mag.

At a distance of 5 kpc with our limiting magnitude, an extinction of  $A_V = 9$  limits us to G4 and earlier stars, while  $A_V = 15$  limits us to F0 and earlier. We select  $A_V = 10$  and G2 as our limits; stars with higher extinction or later spectral type cannot be detected over the entire range of mass or extinction included and thus

are excluded. Approximately 34 stars have a higher extinction than this, including five with extreme calculated extinctions ( $A_V > 50$ ) that most likely suffer from poor photometry and have unrealistic colors. This extinction limit will also have the effect of excluding stars with  $K$ -band excess from the IMF determination, since such sources would appear to be at high extinction. This will tend to push the IMF to flatter values, since lower-mass sources spend more time as IR-excess objects and thus are more likely to be ruled out by this criterion. However, we consider this to be a better approach than including the sources since: 1. the number of sources detected in all three bands in this cluster showing near-IR excess is small, suggesting such sources will not significantly influence the mass; 2. the majority are of a low enough mass to fall below the completeness limit, and are thus excluded anyway regardless of the method; 3. including them (since not all sources are detected in  $J$ ) would weaken the extinction limit and tend to again force the IMF to flatter values. In clusters where IR-excess sources dominate we do not fit an IMF (see Section 3.2.1 for further discussion).

Individual extinctions are derived by moving the stars along the direction of the reddening vector until they lie on the ZAMS. Once the stars have been corrected individually for extinction, they are placed in mass bins. We fit a power law to the data, excluding masses  $< 1.1M_\odot$  from the fit since they cannot be seen over the entire range of extinctions in the cluster. The IMF slope we derive by this method is  $\Gamma = -1.61 \pm 0.2$ . As for the KLF method, the quoted errors represent only the formal errors in the fit and should be considered an underestimate.

The difference between these two values for the IMF emphasizes that formal statistical errors significantly underestimate the true uncertainties in the IMF. In this case, as was the case in Leistra et al. (2005), the CMD method gives a noticeably flatter result than the KLF method. Clearly the individual extinction correction leads to the conclusion that more massive stars are present than an average correction does. This could be due to the effects of mass segregation, or to an incorrectly chosen extinction limit (so that we truly are sampling massive stars more completely than lower mass stars). It is difficult to understand which of these effects is most important without obtaining spectra for a significant number of stars in the cluster.

This cluster is also analyzed by Porras et al. (1999), who use a slightly different distance (5.8 kpc) and extinction ( $\langle A_V \rangle = 5.3 \pm 3.7$ ) and derive an IMF slope of  $\Gamma = -0.59$  based on 54 sources using the  $J$  vs  $J-H$  CMD to individually correct extinctions and compare with a theoretical JLF. This is a significant discrepancy from our result with either method. A number of factors may contribute to this difference. The most significant, however, is likely to be due to a different choice of cluster boundaries. Their quoted cluster radius corresponds to only  $50''9$ , compared to ours of  $\sim 80''$ . This suggests that their IMF will be more weighted toward the cluster core than ours. The value they quote for a field + cluster IMF is  $\Gamma = -2.71 \pm 0.24$ , much steeper and in fact quite close to the value we obtain using the KLF. If the cluster suffers from mass segregation, as we would expect given that it is observed even in very young clusters (e.g. the

Arches cluster (Stolte et al. 2002)), we expect the core IMF to be quite flat. When we re-derive the IMF for this cluster using their radius with our data, we derive an IMF of  $\Gamma = -1.55 \pm 0.22$ , statistically indistinguishable from our original result. Porras et al. (1999) do not comment on issues of confusion or field star contamination, so we cannot evaluate how much of an effect it is likely to have on their result; we expect crowding to be a more significant issue, and a misidentification of blended sources as single stars by Porras et al. (1999) could account for their finding a steeper IMF than we do using the same method.

### 3.2. IRAS 06058+2158 Cluster

We present a three-color composite of the cluster near the IRAS source 06058+2138 in Figure 6. Bik et al. (2005) obtained VLT spectra in  $K$  of several NIR point sources near the IRAS point source, which is located near the center of the cluster, and identified two candidate massive YSOs and an embedded early-B star. The spectrophotometric distance they derive from the B star is 1.0-1.5 kpc. This cluster is much more heavily embedded than the Sh 2-217 cluster, with significant nebular emission and prominent dust lanes. Numerous OH and methanol masers have been detected in this region, which along with the IRAS point source suggest ongoing star formation. (see, e.g., Caswell et al. (1995), Szymczak et al. (2000)). A peak in the  $8 \mu\text{m}$  emission is observed in the MSX data, extending from the region of NIR nebulosity to the southeast to the isolated bright source.

The embedded cluster here is described in the compilation of Lada & Lada (2003), who quote a distance of 1.5 kpc (Carpenter et al. 1993). However, Hanson, Luhman, & Rieke (2002) describe a UCHII region associated with the IRAS point source, and quote a distance of 2.2 kpc (Kömpe et al. 1989), and Bik et al. (2005) obtain a spectroscopic distance of 1.0-1.5 kpc. With no *a priori* reason to prefer one distance over the other, and no uncertainties associated with either, we use the average distance of 1.5 kpc for our analysis.

#### 3.2.1. The KLF

We present color-color and color-magnitude diagrams for this cluster in Figures 7 and 8. The ‘‘cluster region’’ was defined to coincide with the extent of the near-IR nebulosity, and field stars were statistically corrected as described in 3.1. The CMD shows objects spanning a range of extinctions, with relatively few objects with colors consistent with unextincted main-sequence stars remaining in the statistically corrected data. Since the cluster in this case did not fill the field of view, we were able to use the data from the non-cluster portions of the region as our field, eliminating the need for an off-source 2MASS field and extrapolation based on the KLF. The  $J-H$  vs.  $H-K$  color-color diagram shows that the majority of sources in the cluster region exhibit  $K$ -band excess and fall in the region populated by reddened CTTS and YSOs, suggesting they may be pre-main-sequence objects. Because the amount of  $K$ -band excess is affected by many factors (see, e.g., Meyer, Calvet, & Hillenbrand (1997)), deriving masses for these objects is difficult. We thus derive only a KLF for this cluster, and do not convert it to an IMF or derive an IMF from the CMD. We

determine and correct for our incompleteness as in 3.1. The KLF we derive using a statistically-corrected sample of all sources detected in  $K$ , with no attempt to correct for extinction due to the uncertainty of the intrinsic  $H - K$  color of the YSOs that are present, has a slope of  $0.30 \pm 0.03$ . If only sources detected in  $H$  are included, the KLF declines for  $K > 14.5$  since the high extinction means the fainter objects are less likely to be detected in  $H$ .

### 3.2.2. Pre-Main-Sequence Objects

A total of 37 out of 58 sources (63%) detected in all three bands show a K-band excess in the color-color diagram, suggesting they are pre-main sequence objects. This is a lower limit on the actual pre-main-sequence fraction of the cluster, since objects with a sufficiently high IR excess may be detected in  $K$  but not in  $J$  or  $H$ . A total of 49 sources were detected in  $K$  within the cluster region that were undetected in  $J$ ,  $H$ , or both. Adding in these sources would give a PMS fraction of 80%. The latter figure is an upper limit, since some of the  $K$ -only detections are likely to be knots of nebular Br  $\gamma$  emission or heavily extinguished background stars. Comparing these values to the near-IR excess fraction of embedded clusters of known ages presented in Haisch, Lada, & Lada (2001), we conclude that the age of the IRAS 6058 cluster is less than 3 Myr.

We observe a few sources with colors even redder than the reddened extension of the CTTS locus. Meyer, Calvet, & Hillenbrand (1997) observe sources with similar colors, and suggest re-radiation by an extended envelope as an explanation.

### 3.3. IRAS 06104+1524 Cluster

The near-IR cluster image (Figure 9) of the cluster near IRAS 06104+1524 shows a clear separation into two subclusters separated by  $\sim 2'$ . The southwest subcluster is dominated by two closely spaced bright sources while the northeast subcluster is denser and is not dominated by a single object. A ridge of marginally higher density than the surrounding field appears to lie between the subclusters, though it is not apparent whether this is a real feature. The MSX  $8 \mu\text{m}$  image similarly shows two separate peaks, with no indication of a connection. These are treated as separate clusters by Bica et al. (2003), and there are IRAS point sources associated with each of them (IRAS 06104+1524 and IRAS 06103+1523, respectively). The IRAS point sources both have kinematic distances of 3.5 kpc (Wouterloot & Brand 1989), suggesting the subclusters are related. The radio kinematic distances derived to the two sources are the same, and the angular separation is comparable to the size of either subclump; in addition, a slight overdensity of stars can be seen in the  $K$  image. These factors suggest that, at the very least, these clusters are related; they may differ in age, but they are likely to be part of the same general star-formation event. We see no difference between the two apparent in either the CMD or the color-color diagram (Figures 10 and 11); if they do differ in age, it is beyond the ability of our data to discern. Due to this apparent association and the small number of stars in each cluster, we analyze the two together as a single cluster. The CMD after statistical correction and adjusting to a

distance of 3.5 kpc (Wouterloot & Brand 1989) is shown in Figure 12.

Using the color-magnitude diagram based method of deriving an IMF as described above, for a limiting extinction of  $A_V = 25$ , we find an IMF slope of  $\Gamma = -0.9 \pm 0.25$ . Using the KLF method (with no extinction correction, to mimic the results of a study with only single-color photometry available) we arrive at  $\Gamma = -2.6 \pm 0.3$ . Even after allowing for the errors to be larger than quoted due to uncertainty in the photometry and the conversion to mass, these two slopes are inconsistent with each other, suggesting that systematic effects in one or both methods dominate over the statistical errors.

### 3.4. Sh 2-288

The near-IR cluster image (Figure 13) of the cluster near Sh2-288 shows a cluster with a dense core, crossed near the center by a dust lane. The center of the cluster is unresolved in our images, taken with a seeing of  $0.7''$ . This region was previously identified as an embedded cluster by (Dutra & Bica 2001). In their catalog of outer-Galaxy HII regions, Rudolph et al. (1996) quote widely disparate distances, with a radio kinematic distance of 7.2 kpc and a photometric distance of 3.0 kpc (Brand & Blitz 1993). The kinematic distance would make the sources we observe (several with  $K < 12$ ) extremely massive, it is thus far more likely that the photometric distance is correct, and we have used the photometric distance for our analysis.

The  $8 \mu\text{m}$  image from the MSX mission shows a peak coincident with the near-IR nebulosity; there is not a significant amount of  $8 \mu\text{m}$  emission from regions dark in the NIR. This suggests that there are not a significant number of sources so deeply embedded that they cannot be seen in  $K$  present in this cluster.

The  $K$  versus  $H - K$  color-magnitude diagram of the cluster near the HII region Sh2-288 (Figure 14) clearly shows the effects of variable extinction; the stars separate into two groups, one nearly unextinguished and one with  $\sim A_V = 5$ . We correct for field star contamination using the region of the field outside the cluster region as described above. The  $J - H$  versus  $H - K$  color-color diagram (Figure 15) shows few stars separated from the main sequence locus by more than  $2\sigma$ , suggesting that most stars in this cluster are on the main sequence. Extreme outliers in the color-color diagram were inspected individually; in general, they lie in the crowded central region of the cluster and most likely suffer from poor photometry due to the different PSFs in  $H$  and  $K$  that resulted from variations in seeing. Such sources were excluded from analysis of the KLF and the IMF. Additionally, the brightest source in the cluster, which lies in the most crowded central region and has a FWHM slightly broader than most sources in the field, was excluded since it is quite likely to be a blend of multiple sources. We consider that the effects on the IMF are likely to be worse if a blend is included than if any single star, even the most massive, is excluded.

Using the photometric distance of 3.0 kpc from (Rudolph et al. 1996), we derive an IMF from the KLF of  $\Gamma = -1.95 \pm 0.62$ . To better compare the two methods of deriving the IMF, we included only those sources which were also detected in  $H$ , so that the same dataset would be used for both the KLF and CMD methods of deriv-

ing the IMF. We individually de-reddened sources in the  $H - K$  CMD until they were on the main sequence, imposing an extinction limit as before, and derive an IMF of  $\Gamma = -1.62 \pm 0.65$ . Given the large uncertainties, these results are entirely consistent. The better agreement may be because the extinction bias is less in the latter case.

### 3.5. Comparison of Methods for IMF Determination

A summary of the IMFs derived for the three clusters without significant numbers of pre-main-sequence stars and the similar results from (Leistra et al. 2005) is shown in Table 1. In each case, there is a significant difference between the IMF derived from the KLF and that derived from the CMD. Does this reflect only uncertainties, or is one method in general more reliable than the other? A simple analysis would suggest that the CMD method is more reliable, simply because it uses more information; the extinction clearly varies across many embedded clusters (of those analyzed here, most notably Sh 2-288 and IRAS 06058+2158), and accounting for this should provide a more robust estimate of the true IMF. We cannot say for certain that this is the case, however, without obtaining spectra for most of the stars in each cluster, so that we can classify them spectroscopically and obtain individual masses. We note that in each case, the IMF we derive from the CMD by individually correcting the extinction for each object is flatter than that we derive from the KLF by assuming a single extinction for the entire cluster. This suggests that more massive stars may preferentially lie in more heavily extinguished regions in embedded clusters. Resolving this seeming discrepancy would require spectra for a large number of cluster members, so that the IMF derived from spectral classification of stars can be compared to that derived via the different photometric methods.

We examine the relation between derived mass and extinction (with the extinction limit imposed) for the Sh2-217 cluster, where we have the most data, in Figure 16. Such a relation appears to be present, albeit at low significance. This effect is opposite in sign to what would be expected from massive stars clearing their immediate environment more rapidly than their lower-mass counterparts, but the stars we observe are mostly of intermediate mass, rather than truly high mass, such that their winds are not as significant; the effects of mass segregation, placing the more massive stars at denser regions in the cluster, appear to dominate over the effects of clearing in these clusters. Since the clusters are numerically dominated by low-mass stars, the average extinction will be mostly determined by the average for the low-mass stars, changed slightly by the average for high-mass stars. If more massive stars are indeed preferentially found at higher extinction as our results suggest, this would mean the majority of (low-mass) stars are over-corrected for extinction by a small amount when using a single value, while a few (high-mass) stars are under-corrected (thus lowering the derived mass) by a large amount; thus, the effects of over-correcting and under-correcting extinction do not fully cancel out, since the large under-corrections would be more likely to move stars between mass bins than the small over-corrections. If there is no relation between mass and extinction, we would expect these two results to cancel, since the average extinction for low-mass stars would be the same as that for high-mass stars.

## 4. SUMMARY

We present NIR images of four embedded clusters in the outer Galaxy. In the case of the cluster near IRAS 06058+2158 the number of stars with NIR excess indicates a pre-main-sequence fraction between 60% and 80% and an age of less than 3 Myr; the other three clusters show less nebular emission and fewer stars with NIR excess indicating an older age. We compute the IMF for the three clusters dominated by main-sequence stars, in each case using both a KLF-based method relying on a single extinction value for the cluster and using only  $K$  band data and a CMD-based method where an individual extinction value is calculated for each star. We found a statistically significant difference between the two values in two of the three cases, prompting us to examine IMF values of embedded clusters from the literature to determine whether systematic effects are at work. We found a significant difference in the mean value of the IMFs for embedded clusters derived from methods that handle extinction individually compared with those that adopt a single value for the extinction. Although a larger sample would help to make this claim more robust, since many of the results come from a single study (Porrás et al. 1999) and methodological details of that work could affect the results, we consider it to be significant enough that IMFs obtained by different methods should not be compared in an attempt to search for variations in the IMF from region to region.

Truly reliable IMFs for embedded clusters will most likely require spectra for a large number of stars in the clusters; we are continuing to try to obtain spectra for these sources to better characterize the massive star population and the IMF of these clusters.

We thank Don McCarthy for use of and assistance with the PISCES instrument. We thank Phil Massey and Michael Meyer for comments that improved this paper. This research has made use of the SIMBAD database, operated at CDS, Strasbourg, France. This publication

makes use of data products from the Two Micron All Sky Survey (2MASS), which is a joint project of the University of Massachusetts and IPAC, funded by NASA and NSF.

## REFERENCES

- Bessell, M. S. & Brett, J.M. 1988, *PASP*, 100, 1134  
 Bica, E., Dutra, C.M., Soares, J., & Barbuy, B. 2003, *A&A*, 404, 223  
 Bik, A., Kaper, L., Hanson, M.M., & Smits, M. 2005, *A&A*, 440, 121  
 Blum, R. D., Conti, P. S., & Daminieli, A. 2000, *AJ*, 119, 1860  
 Blum, R. D., Daminieli, A., & Conti, P. S. 2001, *AJ*, 121, 3149  
 Borissova, J., Ivanov, V. D., Minniti, D., Geisler, D. & Stephens, A. W. 2005, *A&A*, 435, 95  
 Brand, J. & Blitz, L. 1993 *A&A*, 275, 67  
 Caswell, J. L., Vaile, R. A., & Forster, J. R. 1995, *MNRAS*, 277, 210  
 Carpenter, J. M., Snell, R. L., Schloerb, F. P., & Skrutskie, M. F. 1993, *ApJ*, 407, 657  
 Comerón, F., Rieke, G. H., & Rieke, M. J. 1996, *ApJ*, 473, 294  
 Cotera, A. S., Erickson, E. F., Colgan, S. W. J., Simpson, J. P., Allen, D. A., Burton, M. G. 1996, *ApJ*, 461, 750  
 Deharveng, L., Zavagno, A., Salas, L., Porras, A., Caplan, J., & Cruz-Gonzalez, I. 2003, *A&A*, 399, 1135  
 Dutra, C. M. & Bica, E. 2000, *A&A*, 359, 9  
 Dutra, C. M. & Bica, E. 2001, *A&A*, 376, 434  
 Dutra, C. M., Ortolani, S., Bica, E., Barbuy, B., Zocalli, M., & Momany, Y. 2003, *A&A*, 408, 127  
 Elmegreen, B. G., Efremov, Y., Pudritz, R. E., & Zinecker, H. 2000, in *Protostars & Planets IV*: University of Arizona Press; eds. Mannings, V., Boss, A. P., & Russell, S. S., 841  
 Figier, D. F., Morris, M., & McLean, I. S. 1996, in *The Galactic Center: Astronomical Society of the Pacific Conference Series*; ed Grebel, R., 263  
 Figier, D. F., Kim, S. S., Morris, M., Serabyn, E., Rich, R. M., & McLean, I. S. 1999, *ApJ*, 525, 750  
 Figuerêdo, E., Blum, R. D., Daminieli, A., & Conti, P. S. 2002, *AJ*, 124, 2739  
 Figuerêdo, E., Blum, R. D., Daminieli, A., & Conti, P. S. 2005, *AJ*, 129, 1523  
 Haisch, K. E., Lada, E. A., Lada, C. J. 2001, *ApJ*, 553, 153  
 Hanson, M. M., Conti, P. S., & Rieke, M. J. 1996, *ApJS*, 525, 750  
 Hanson, M. M., Luhman, K. L., & Rieke, G. H. 2002, *ApJS*, 138, 35  
 Hillenbrand, L. A., Massey, P., Strom, S. E., & Merrill, M. K. 1993, *AJ*, 106, 1906  
 Homeier, N. L., & Alves, J. 2005, *A&A*, 430, 481  
 Ivanov, V. D., Borissova, J., Pessev, P., Ivanov, G. R. & Kurtev, R. 2002, *A&A*, 394, 1  
 K mpe, C., Baudry, A., Joncas, G., & Wouterloot, J. G. A. 1989, *A&A*, 221, 295  
 Lada, C. J., Alves, J., & Lada, E. A. 1996, *AJ*, 111, 1964  
 Lada, C. J. & Lada, E. A. *ARA&A*, 41, 57  
 Leistra, A., Cotera, A. S., Liebert, J. & Burton, M. 2005, *AJ*, 130, 1719  
 Malagnini, M. L., Morossi, C., Rossi, L. & Kurucz, R. L. 1986, *A&A*, 162, 140  
 Massey, P., Johnson, K. E., & DeGioia-Eastwood, K. 1995, *ApJ*, 454, 151  
 Massey, P. 2003, *ARA&A*, 41, 15  
 McCarthy, D.W., Ge, J., Hinz, J.L., Finn, R.A., & deJong, R.S. 2001, *PASP*, 113, 353  
 Meynet, G. & Maeder, A. 2003, *A&A*, 404, 975  
 Meyer, M. R., Calvet, N., & Hillenbrand, L. A. 1997, *AJ*, 114, 288  
 Muench, A.A., Lada, E.A., & Lada, C.J. 1999, in *33rd ESLAB Symposium, Star Formation from the Small to the Large Scale*, eds. F. Favata, A. Kass, & A. Wilson, 301  
 Nagata, T., Woodward, C. E., Shure, M., & Kobayashi, N. 1995, *AJ*, 109, 1676  
 N rnberger, D. E. A., & Petr-Gotzens, M. G. 2002, *A&A*, 382, 537  
 Okumura, S., Atsushui, M., Nishihara, E., Watanabe, E., & Yamashita, T. 2000, *ApJ*, 543, 799  
 Porras, A., Cruz-Gonzalez, I., & Salas, L. 1999, in *33rd ESLAB Symposium, Star Formation from the Small to the Large Scale*, eds. F. Favata, A. Kass, & A. Wilson, 491  
 Porras, A., Christopher, M., Allen, L., DiFrancesco, J., Megeath, S.T., & Myers, P.C. 2003, *AJ*, 126, 1916  
 Rudolph, A. L., Brand, J., de Geus, E. J., & Wouterloot, J. G. A. 1996, *ApJ*, 653, 669  
 Scalo, J. 1998 in *The Stellar Initial Mass Function*, ASP Conference Series Vol. 142, eds. G. Gilmore & D. Howell, p. 201  
 Stolte, A., Grebel, E. K., Brandner, W., Figier, D. F. 2002, *A&A*, 394, 459  
 Szymczak, M., Hrynek, G., & Kus, A. J. 2000, *A&AS*, 143, 269  
 Vacca, W. D., Garmany, C. D., & Shull, J. M. 1996, *ApJ*, 460, 914  
 Wegner, W. 1994, *MNRAS*, 270, 229  
 Wouterloot, J. G. A. & Brand, J. 1989, *A&A*, 80, 149

TABLE 1  
IMFs FOR EMBEDDED STELLAR CLUSTERS

Cluster	IMF: Common $A_V$	IMF: Individual $A_V$	Distance (kpc)	Source
Sh2-288	$\Gamma = -1.95 \pm 0.82$	$\Gamma = -1.62 \pm 0.5$	3.0	This work
IRAS 06104+1524	$\Gamma = -2.49 \pm 0.3$	$\Gamma = -1.38 \pm 0.6$	3.5	This work
Sh2-217	$\Gamma = -2.7 \pm 0.25$	$\Gamma = -1.61 \pm 0.2$	5.0	This work
G305.3+0.2	$\Gamma = -1.5 \pm 0.3$	$\Gamma = -0.98 \pm 0.2$	4.0	Paper I

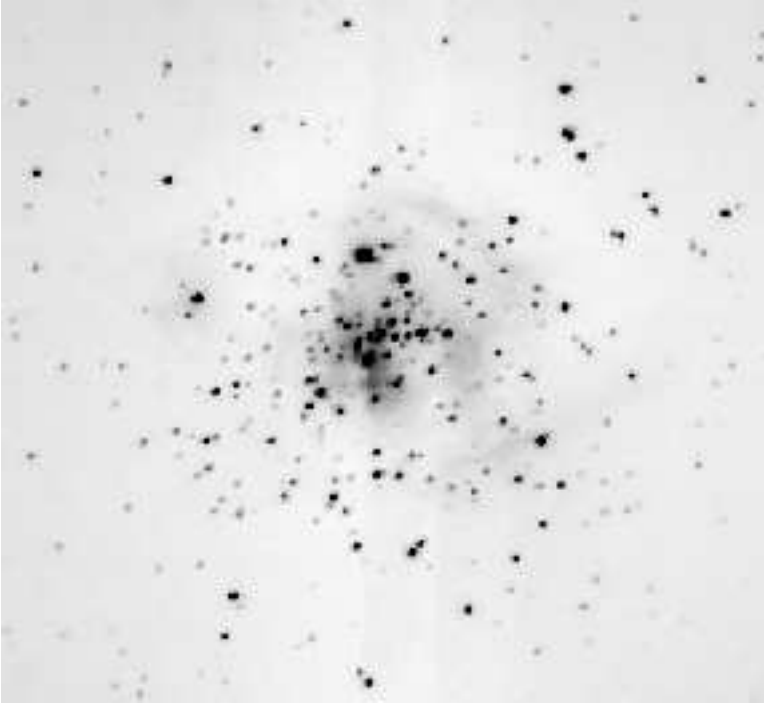


FIG. 1.—  $K$ -band image of the Sh 2-217 cluster center (North=up, East=left). Image is approximately  $120''$  on a side. The stellar density does not plateau in our entire  $3'$ FOV, suggesting the cluster outskirts continue at least to the edge of our image.

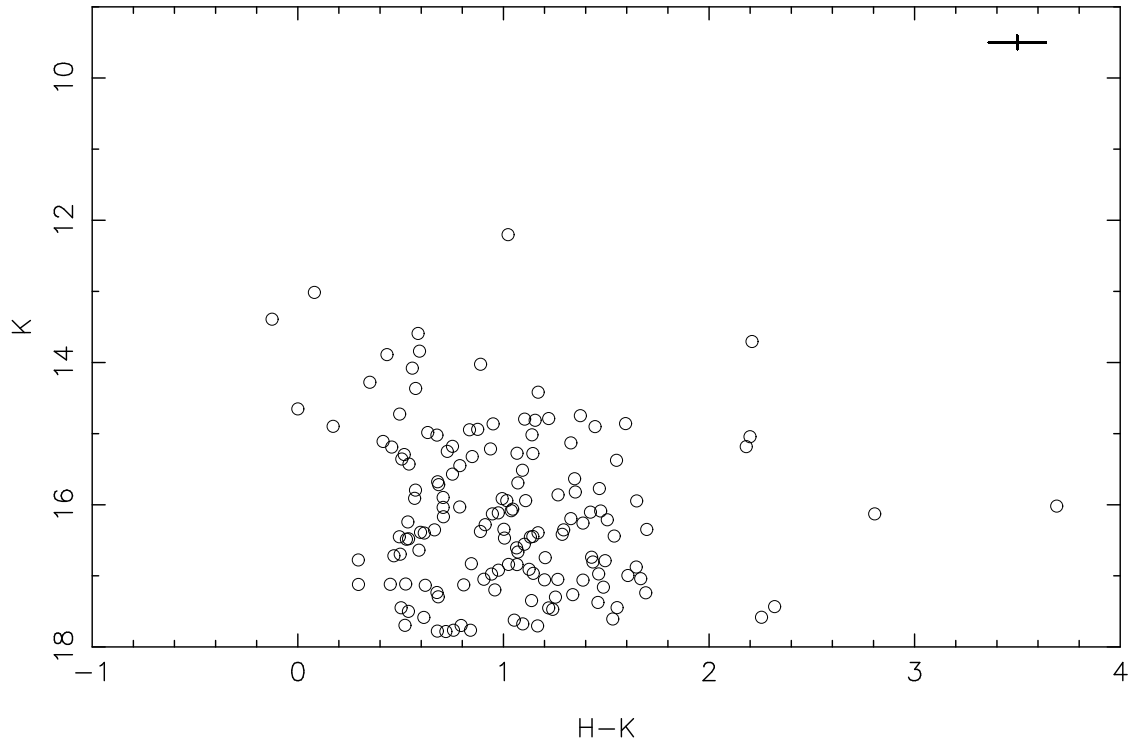


FIG. 2.—  $K$  vs.  $H - K$  color-magnitude diagram for the cluster near Sh2-217. Average DAOPHOT error bar is the size of the plot symbols or smaller. Overall uncertainties including calibration (which include terms that will not affect the relative position of the points) are indicated by the symbol in the upper right.

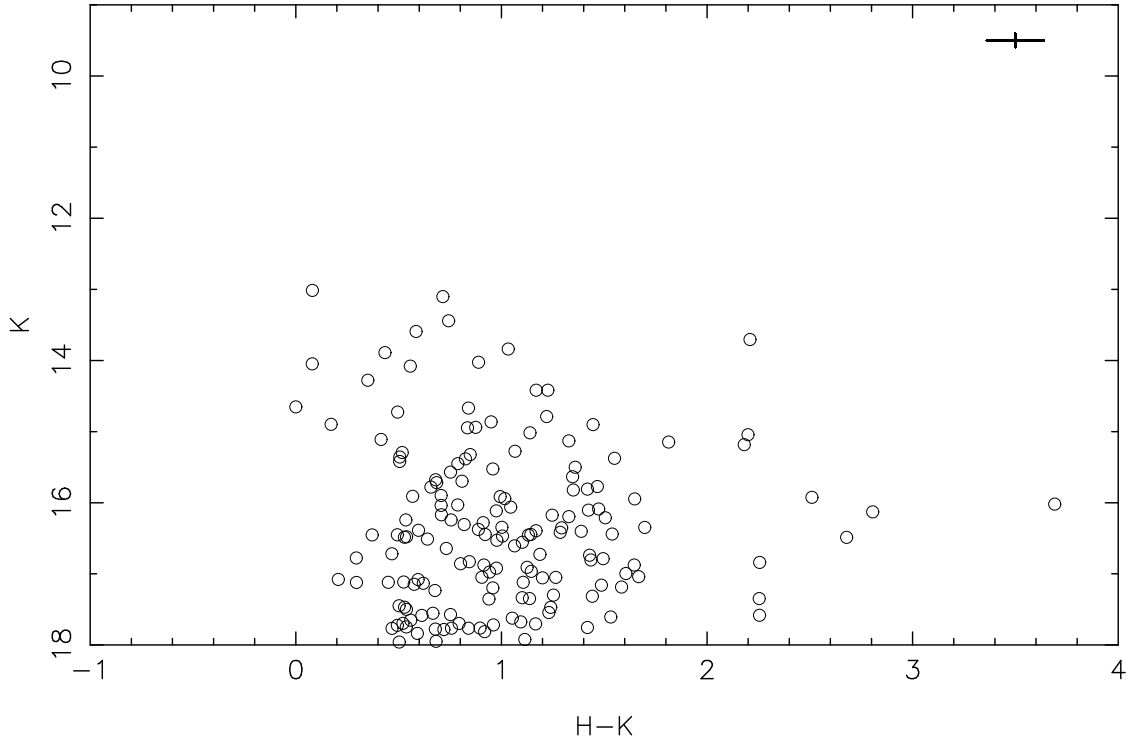


FIG. 3.— Statistically-corrected  $K$  vs.  $H - K$  color-magnitude diagram for the cluster near Sh2-217. Statistical correction was done based on the 2MASS Point Source Catalog for an adjacent field, extrapolating to the our limiting magnitude based on the luminosity function.

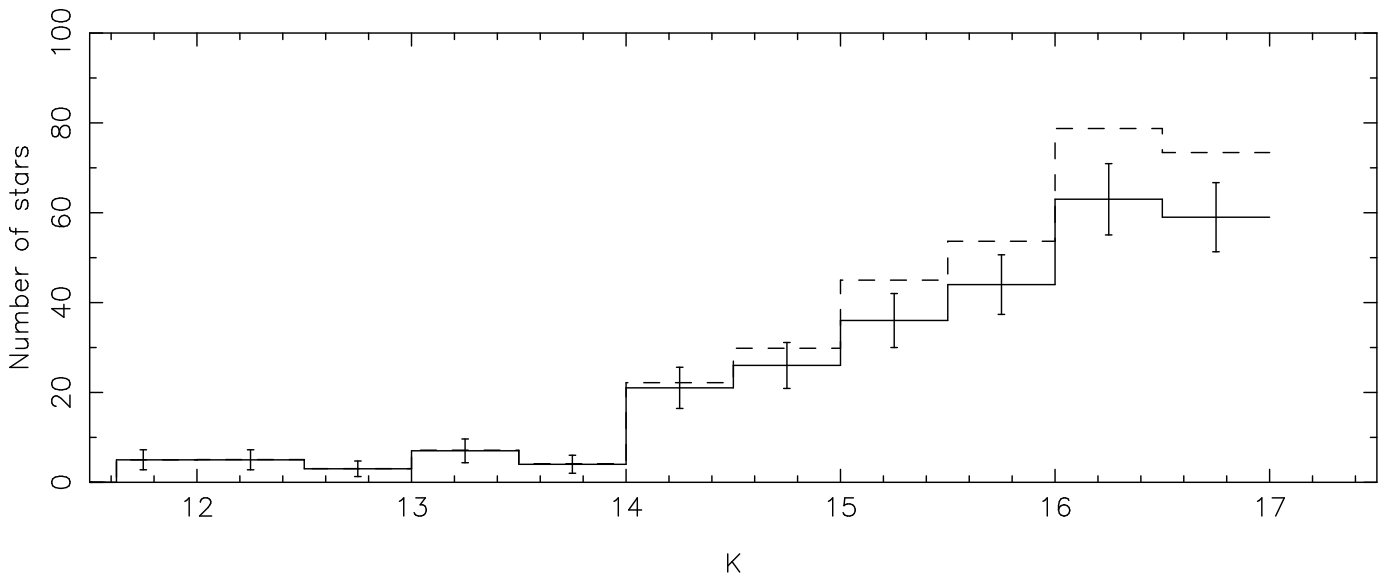


FIG. 4.—  $K$  luminosity function for the Sh2-217 cluster. (Solid is measured; dashed is corrected for incompleteness.) Since the cluster fills the field of view and the comparison 2MASS data do not go as deep, we do not show a field sample for comparison.

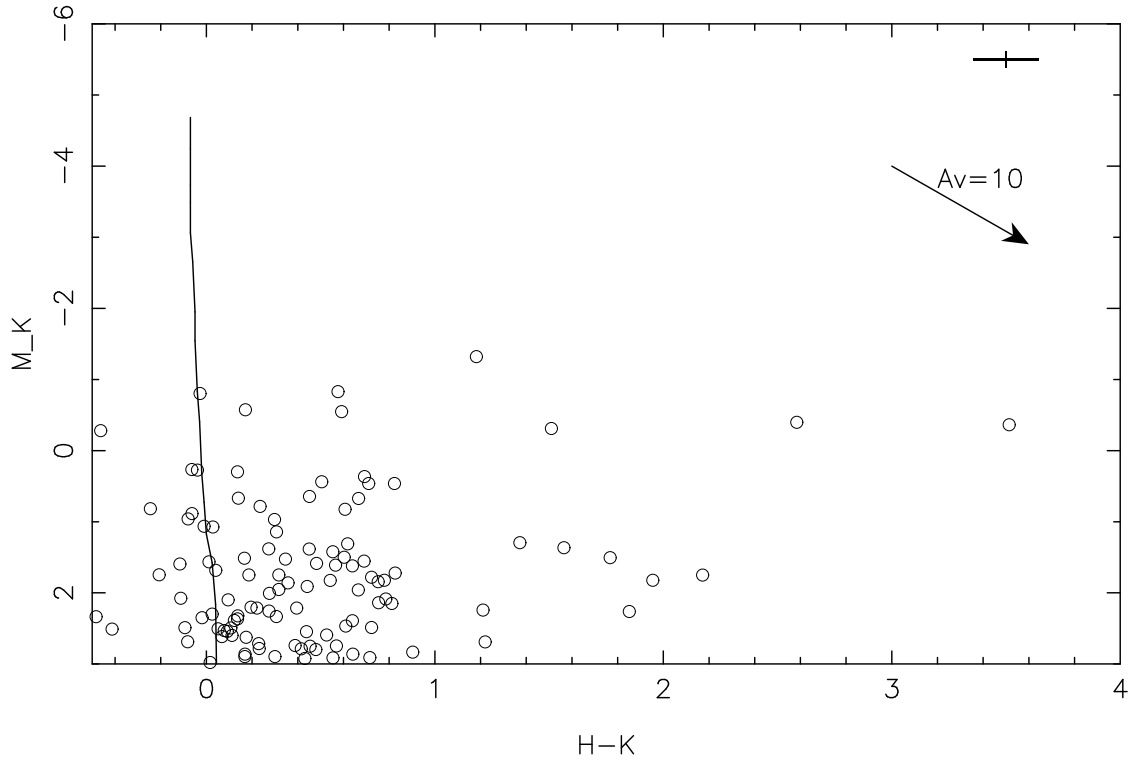


FIG. 5.—  $K$  vs.  $H - K$  color-magnitude diagram for the Sh2-217 cluster adjusted to a distance of 5 kpc. The ZAMS converted to observed quantities as described is overplotted.



FIG. 6.— Color composite ( $J =$  blue,  $H =$  green,  $K =$  red) of the IRAS 06058+21 cluster region (North=up, East=left). Image is approximately  $140''$  on a side.

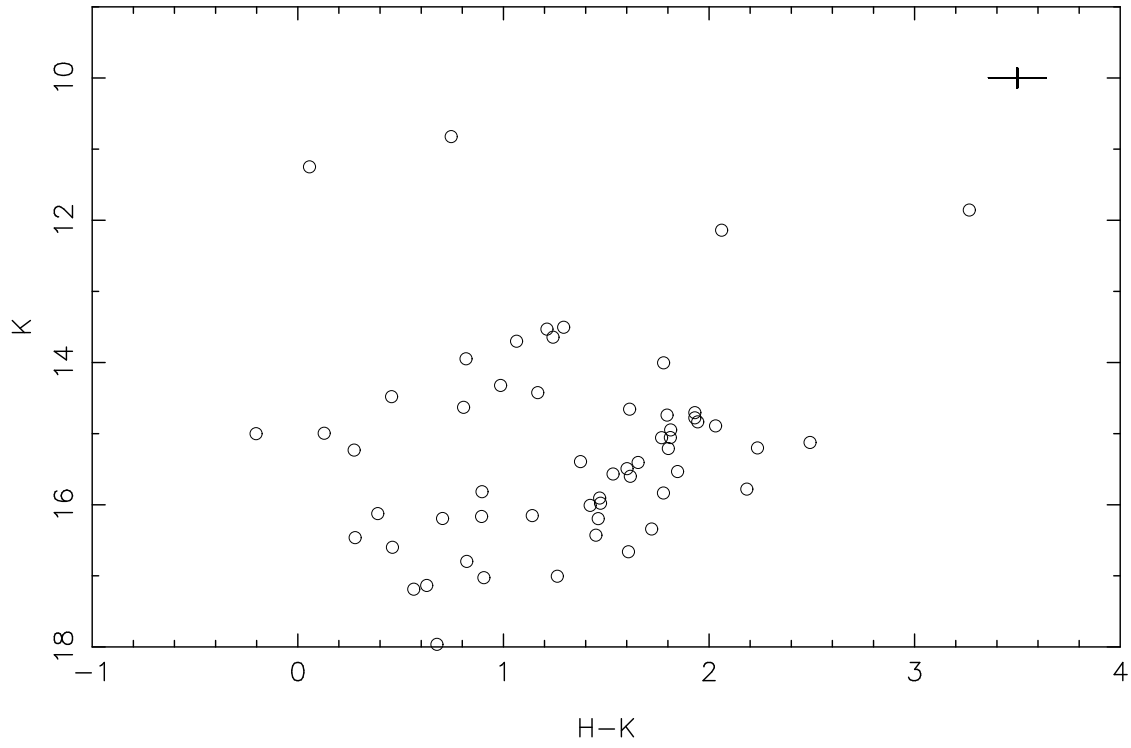


FIG. 7.— Statistically field-star corrected  $K$  vs.  $H - K$  color-magnitude diagram for the cluster near IRAS 06058+2158. Significant and variable extinction is evident in this cluster. Typical errorbars are the size of the plot symbols. Overall uncertainties including calibration (which include terms that will not affect the relative position of the points) are indicated by the symbol in the upper right.

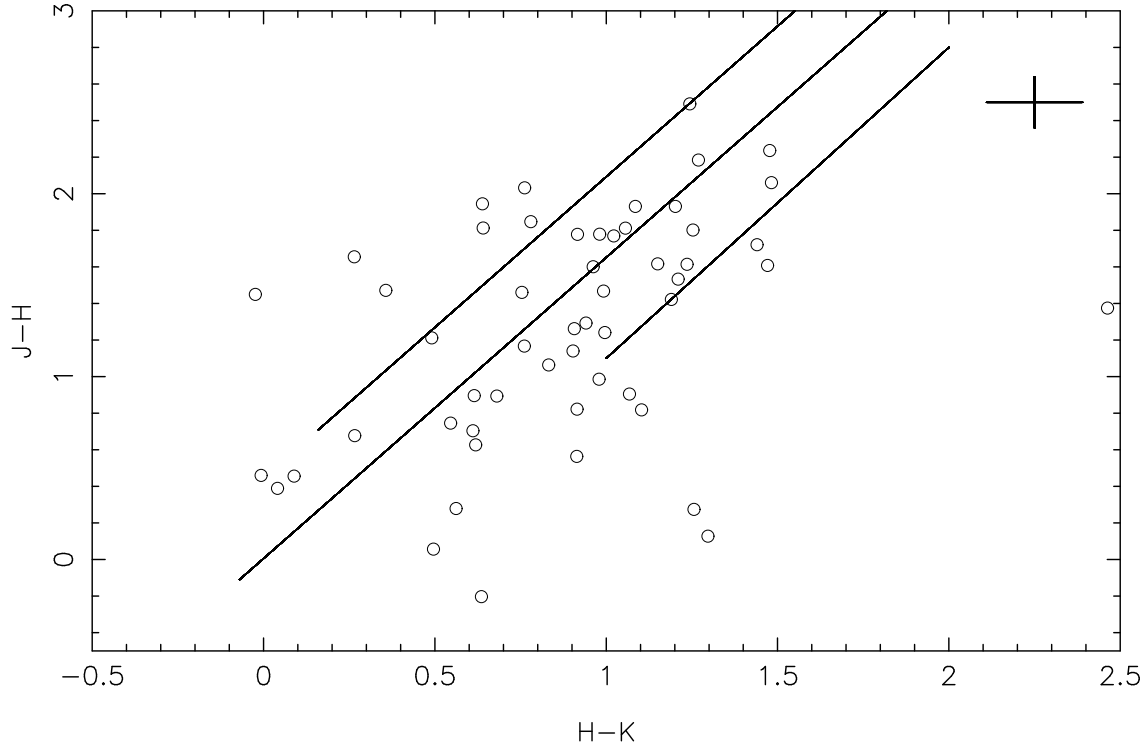


FIG. 8.—  $J - H$  vs.  $H - K$  color-color diagram for the cluster near IRAS 06058+2158. The lines (parallel to the reddening vector) delineate the possible location of reddened main-sequence stars. Over half of our sources show  $K$ -band excess; their colors are not consistent with reddened main-sequence sources. Typical errorbars are the size of the plot symbols. Overall uncertainties including calibration (which include terms that will not affect the relative position of the points) are indicated by the symbol in the upper right. Points to the left of the reddening lines lie in crowded regions and may suffer from confused photometry. Points more than  $3\sigma$  to the left of the reddening line were excluded from the IMF determination.



FIG. 9.— Color composite ( $J$  = blue,  $H$  = green,  $K$  = red) of the IRAS 06103+1523 / 06104+1524 cluster(s) (North=up, East=left). Image is approximately  $120''$  on a side.

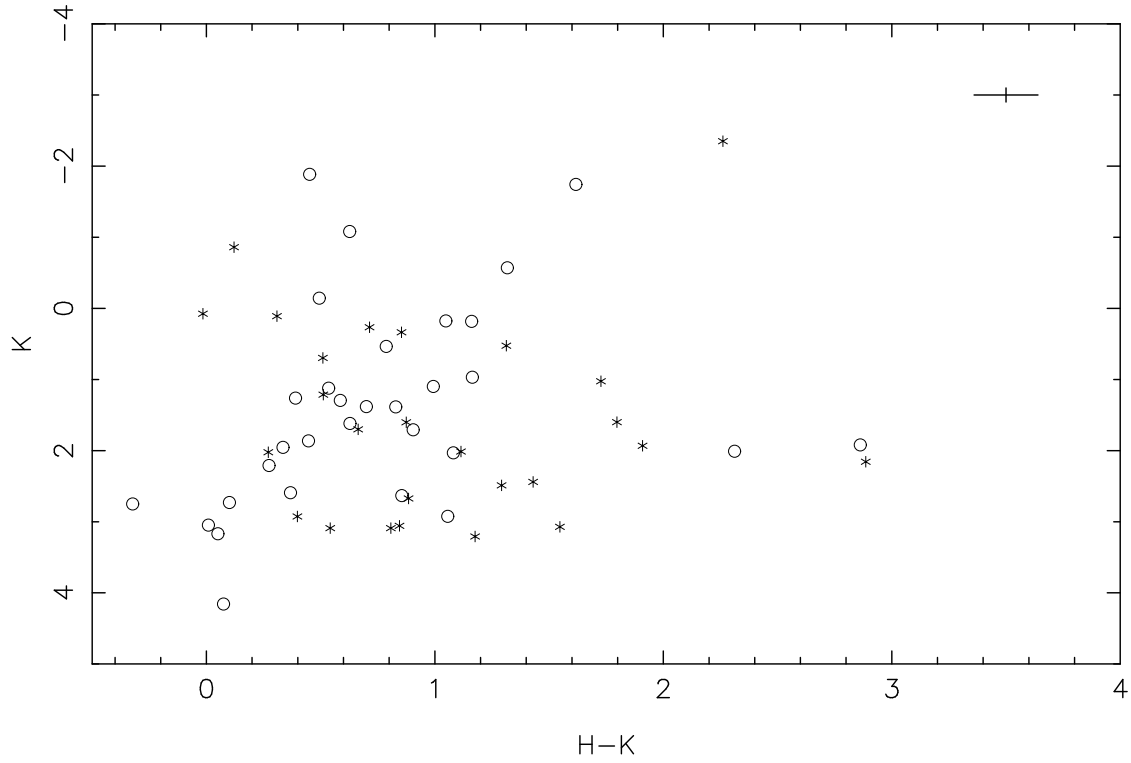


FIG. 10.—  $K$  vs.  $H - K$  color-magnitude diagram for the IRAS 06104+1524 / 06103+1523 cluster(s) adjusted to a distance of 3.5 kpc. *Circles*: NE cluster. *Asterisks*: SW cluster. There is no difference in the CMD apparent for the two clusters, so we treat them as one to improve the statistics. Typical errorbars are the size of the plot symbols. Overall uncertainties including calibration (which include terms that will not affect the relative position of the points) are indicated by the symbol in the upper right.

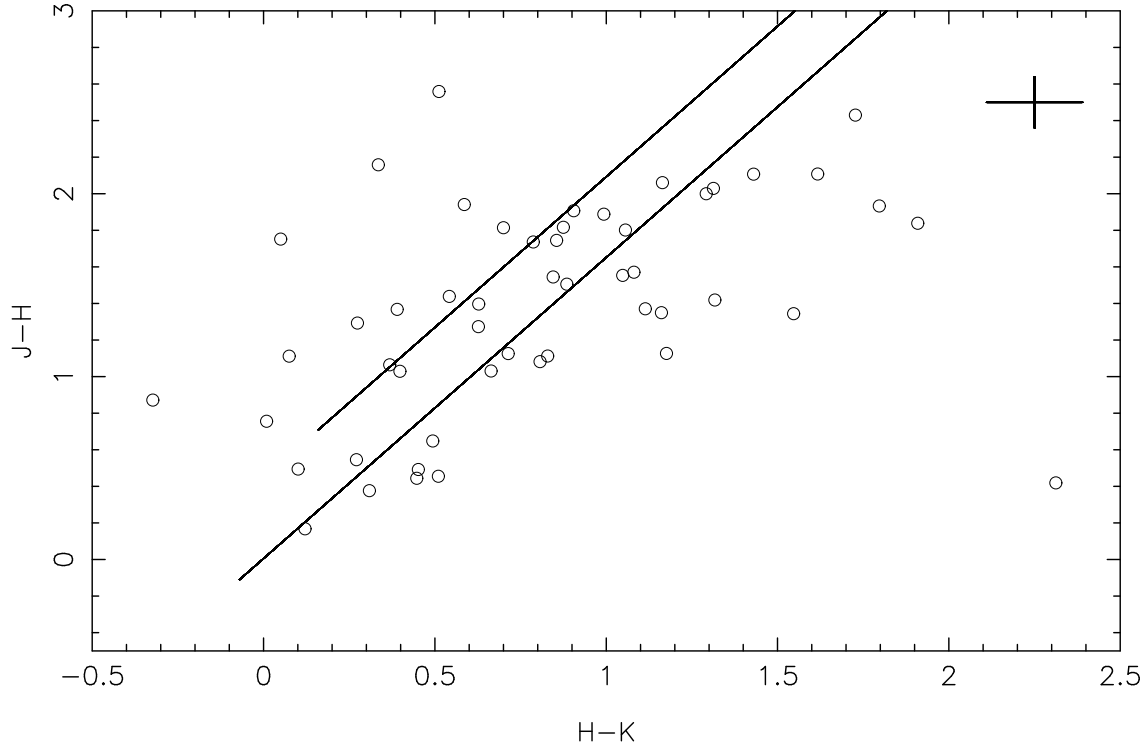


FIG. 11.—  $J - H$  vs.  $H - K$  color-color diagram for the IRAS 06104+1524 / 06103+1523 cluster(s). Typical errorbars are the size of the plot symbols. Overall uncertainties including calibration (which include terms that will not affect the relative position of the points) are indicated by the symbol in the upper right.

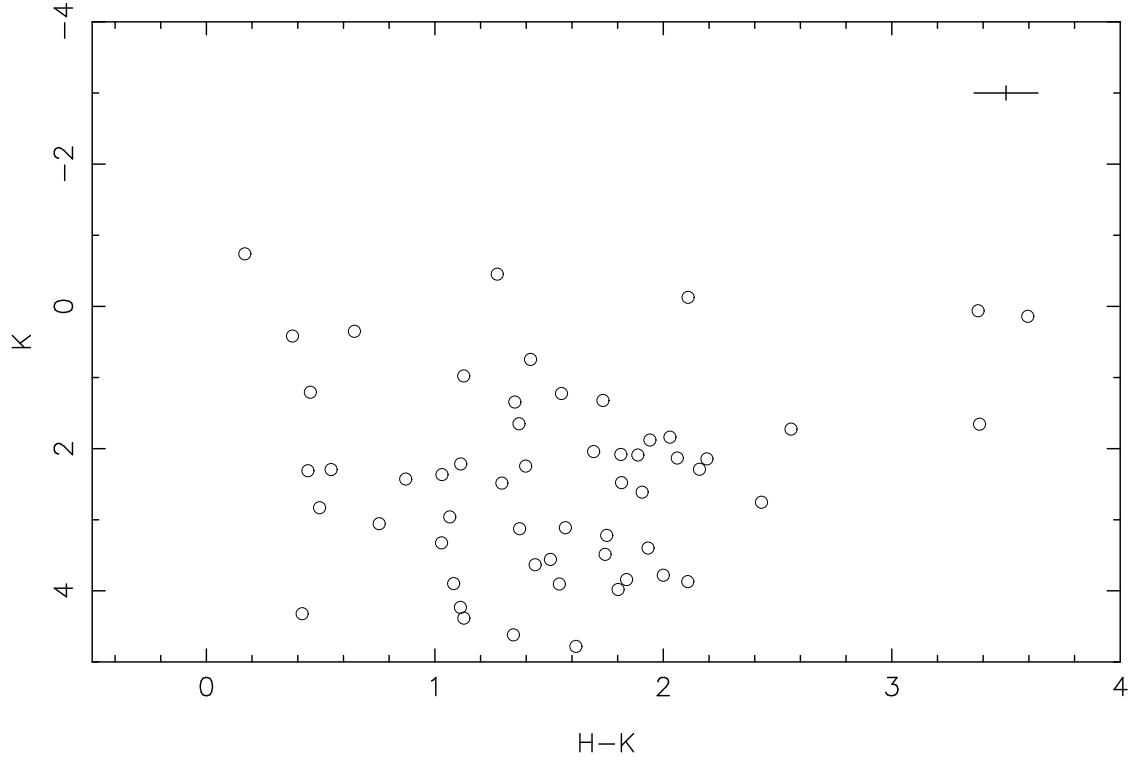


FIG. 12.— Statistically corrected  $K$  vs.  $H - K$  color-magnitude diagram for the IRAS 06104+1524 / 06103+1523 cluster(s) adjusted to a distance of 3.5 kpc. Typical errorbars are the size of the plot symbols. Overall uncertainties including calibration (which include terms that will not affect the relative position of the points) are indicated by the symbol in the upper right.



FIG. 13.— Color composite ( $J$  = blue,  $H$  = green,  $K$  = red) of the Sh 2-288 cluster region (North=up, East=left).

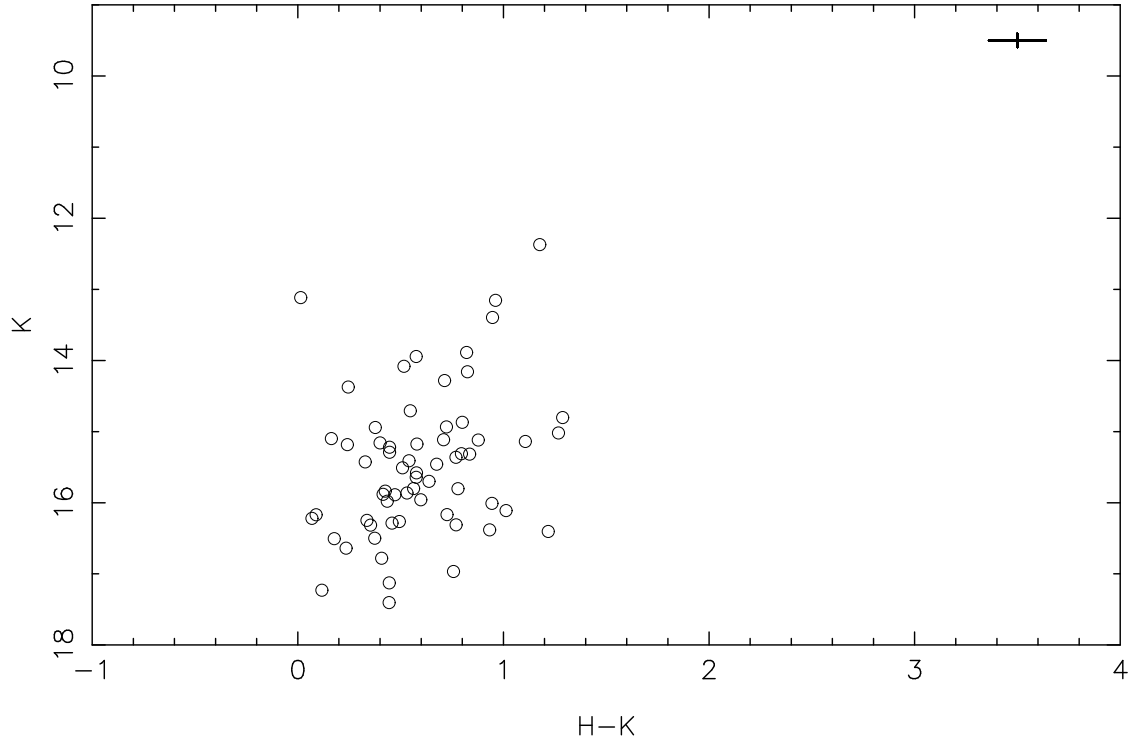


FIG. 14.— Statistically corrected  $K$  vs.  $H - K$  color-magnitude diagram for the Sh2-288 cluster. The bright central source, which we have identified as a blend of two or more stars, has been removed as well. Typical errorbars are the size of the plot symbols. Overall uncertainties including calibration (which include terms that will not affect the relative position of the points) are indicated by the symbol in the upper right.

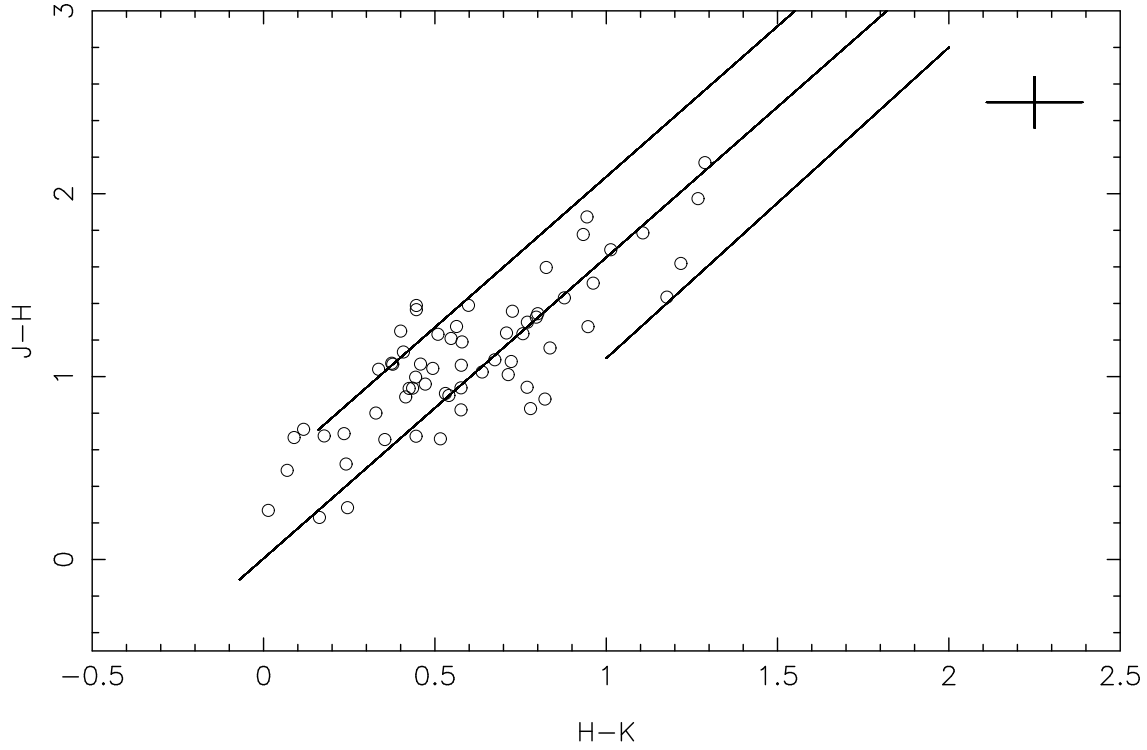


FIG. 15.— Statistically corrected  $J - H$  vs.  $H - K$  color-color diagram of the Sh2-288 cluster. The lines (parallel to the reddening vector) delineate the possible location of reddened main-sequence stars and of reddened T Tauri stars. Typical errorbars are the size of the plot symbols. Overall uncertainties including calibration (which include terms that will not affect the relative position of the points) are indicated by the symbol in the upper right.

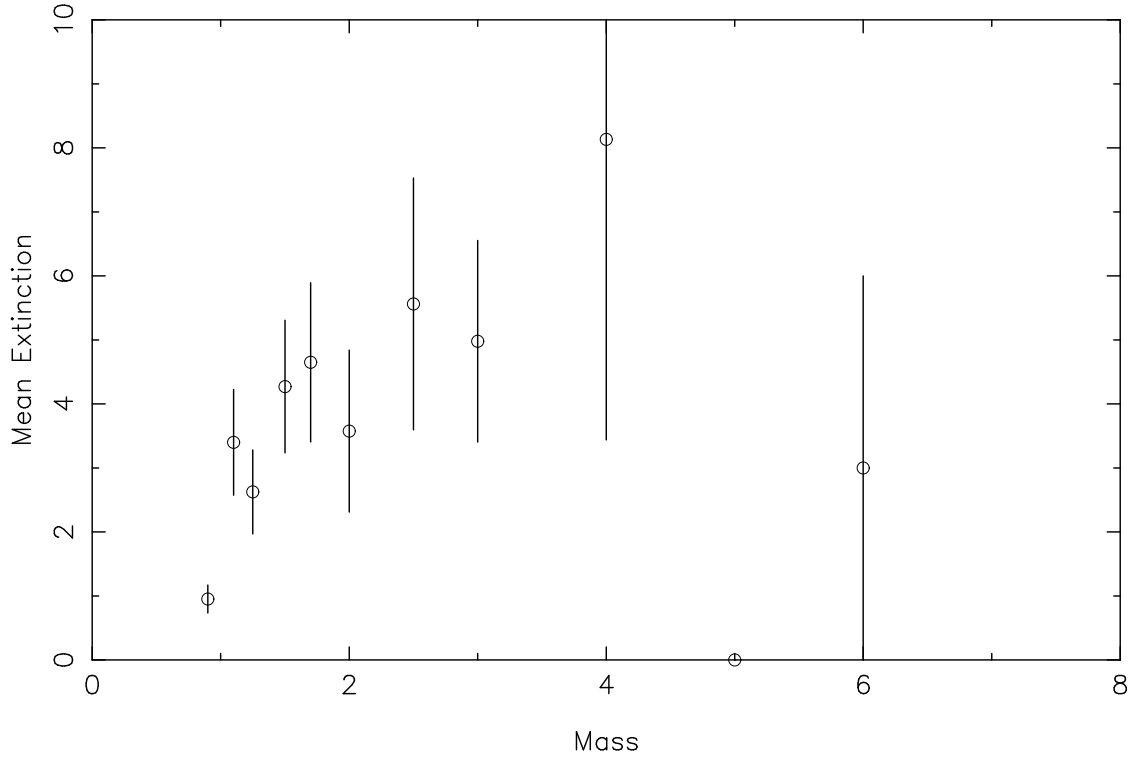


FIG. 16.— Mean extinction derived from  $H - K$  color for sources in each mass bin for the Sh2-217 cluster. An extinction limit of  $A_V = 10$  has been imposed; sources at higher derived extinction are not included in the calculation. More massive sources appear to preferentially lie at higher extinctions, albeit with low significance.